

# Nanostructured Silicon Sensors

*Huseyn M. Mamedov*

## Abstract

Nanostructure porous silicon layers with systematically varied pore size of 8–70 nm were fabricated onto the p-type c-Si wafers using electrochemical anodizing method from HF + ethanol and HF + ethanol + CdCl<sub>2</sub> solutions (hereafter PS and PSCD, respectively). Gas and photo sensors based on c-Si/PS (or PSCD)/CdS and c-Si/PS/Cd<sub>0.4</sub>Zn<sub>0.6</sub>O heterojunctions were synthesized by depositing CdS and Cd<sub>0.4</sub>Zn<sub>0.6</sub>O films onto the c-Si/PS (or PSCD) substrates by electrochemical deposition (ED hereafter). The morphology of the PS and PSCD layers, CdS, and Cd<sub>0.4</sub>Zn<sub>0.6</sub>O films was studied using scanning electron microscopy (SEM). Gas- and photosensitivity properties of heterojunctions were studied as a function of pore size. The optimal pore size is determined, which provides the maximum gas- and photosensitivity of heterojunctions in this study. It was established that the heterojunctions based on PSCD possess higher gas- and photosensitivity than heterojunctions based on PS.

**Keywords:** porous silicon, electrochemistry, nanostructure, thin film, photo sensors, gas sensors

## 1. Introduction

Currently, materials prepared by low-temperature electrochemical processing of semiconductors, in particular PS, formed by electrochemical etching of monocrystalline silicon (c-Si) are of particular interest. Anodic polarization of c-Si in hydrofluoric acid solution leads to formation of controlled network of pores of various morphology, size, and orientation. It is generally known that the surface modification of the silicon wafer plays a major role in the sensitivity enhancement of gas and photo sensors [1, 2, 7]. So, the porous surface of silicon layers participates in the processes of light absorption, gas adsorption, and desorption.

On the other hand, nanostructured PS has emerged as an attractive material in the field of photoelectronics due to its broadband gap, wide optical transmission range, favorable absorption spectrum, and surface texture. The surface roughness and low effective refractive index which can reduce reflection losses of sunlight radiation are the primary benefits offered by PS over c-Si [3–5]. A highly porous PS layer can enhance the efficiency of solar cells by increasing light trapping in the active region [6], solving the lattice mismatch problem, and surface reflection is also corrected due to the refractive index of silicon as reported by several other authors [7–10].

So, PS has disadvantages, also. The surface of the PS was covered with Si-H<sub>x</sub> bond groups immediately after the deposition. In the process of storage in air, the Si-H<sub>x</sub> bond groups are replaced by Si-O<sub>x</sub> bond groups, and ultimately, silicon nanocrystallites are covered by an amorphous layer which is the main reason for

the instability and degradation of all electrical, photovoltaic, photoluminescent, and sensor devices based on PS. There are various technological methods used for the passivating of the PS surface. For example, in [11], the passivating of PS was performed at the excretory hydrogen plasma. Passivating of PS can also be done by inserting different elements into the matrix. For example, in [12], the authors employed carbohydrate solutions in the PS matrix and then tried to carbide the matrix by thermal annealing. As the authors point out, carbohydrates decompose at a temperature of 2000°C and are converted to carbon and water vapor. Since carbohydrates are not volatile, almost all carbon in them remains in the pores. At this time, the size of the molecules of the selected carbohydrate should be smaller than the size of the pores. The authors have chosen sucrose as a conventional carbohydrate product. In some cases, the process of passage of hydrogen and oxygen in the PS was carried out directly with the deposition process. For this purpose, various salts (AuCl<sub>3</sub>, FeCl<sub>3</sub>, NaNO<sub>2</sub>, KIO<sub>3</sub>, CrO<sub>3</sub>, etc.) were added to the solution in the deposition process [13–18]. In [13, 14], gold and iron chloride salts were added at different concentrations during the dissolution of PS. The main purpose of the study was to replace the non-stable Si-H<sub>x</sub> complexes by Si-Au or Si-Fe stable bonds. It has been established that anodizing in a metallic atmosphere not only stabilizes but also improves the electrical and optical parameters of PS.

Therefore, for the purpose of comparison, the results of investigations of the morphological, electrical, and photoelectrical parameters of heterojunctions p-Si/CdS and p-Si/Cd<sub>0.4</sub>Zn<sub>0.6</sub>O based on PS [19, 20] and PSCD are considered in this chapter.

## 2. Preparation p-Si/PS (or PSCD)/CdS and p-Si/PS (or PSCD)/Cd<sub>0.4</sub>Zn<sub>0.6</sub>O heterojunctions

P-type single-crystal Si wafer with orientation of (100), resistivity of 0.01–2.5 Ohm cm, and thickness of 0.2–0.6 μm was etched through an electrochemical process to produce the porous structure. Before anodizing, the c-Si surface was cleaned from the SiO<sub>2</sub> oxide layer as well as contaminants, in an aqueous solution of hydrofluoric acid (HF), washed with deionized water at a temperature of 80°C and ethyl alcohol, and then dried in air. Anodizing of the c-Si substrate surface was carried out in a Teflon chamber with a platinum cathode [19, 20].

HF:ethanol (1,1) solutions with and without CdCl<sub>2</sub> (aqueous solution of CdCl<sub>2</sub> in 10:1 concentration was added to solution) were used for the formation of porous silicon. The anodizing current was 40–70 mA/cm<sup>2</sup>. Depending on the anodizing time (30–1800 seconds) and potential in solutions, PS layers (prepared from solution without CdCl<sub>2</sub>) and PSCD layers (prepared from solution with CdCl<sub>2</sub>) with the pore sizes of 8–70 nm were prepared on the c-Si surface. For the comparison, electrical and photoelectrical properties of heterojunctions on the base of PS and PSCD layers, prepared at same anode potentials (20, 25, and 30 V), were investigated. After the formation of PS and PSCD layers, the samples were immersed in ethyl alcohol, dried in air, and placed in an electrochemical bath for deposition of nanostructured CdS and Cd<sub>0.4</sub>Zn<sub>0.6</sub>O films.

Electrochemical deposition of CdS and Cd<sub>0.4</sub>Zn<sub>0.6</sub>O films onto the c-Si/PS and c-Si/PSCD substrates was carried out at a temperature of 80°C in an aqueous solution of CdCl<sub>2</sub> + Na<sub>2</sub>S<sub>2</sub>O<sub>3</sub> and Zn(NO<sub>3</sub>)<sub>2</sub> + Cd(NO<sub>3</sub>)<sub>2</sub> (99.5% purities) salts, respectively (**Table 1**) [19–21]. Cyclic voltammetry based on obtaining and decoding the current–voltage dependences of the polarized electrode–electrolyte solution interface was used to control electrochemical reactions in each solution, and then in their combined solution with the same concentration and pH. Cyclic

Samples	Mole fraction of salts (mM)		Deposition current and potential	
	CdS	CdCl <sub>2</sub>	Na <sub>2</sub> S <sub>2</sub> O <sub>3</sub>	J (mA/cm <sup>2</sup> )
	200	50	20	-0.82
Cd <sub>0.4</sub> Zn <sub>0.6</sub> O	Zn(NO <sub>3</sub> ) <sub>2</sub>	Zn(NO <sub>3</sub> ) <sub>2</sub>	J (mA/cm <sup>2</sup> )	U <sub>c</sub> (V)
	5.92	3.95	3.4	-1.2

**Table 1.**  
 Mole fraction of salts and deposition current and potential for the CdS and Cd<sub>0.4</sub>Zn<sub>0.6</sub>O films.

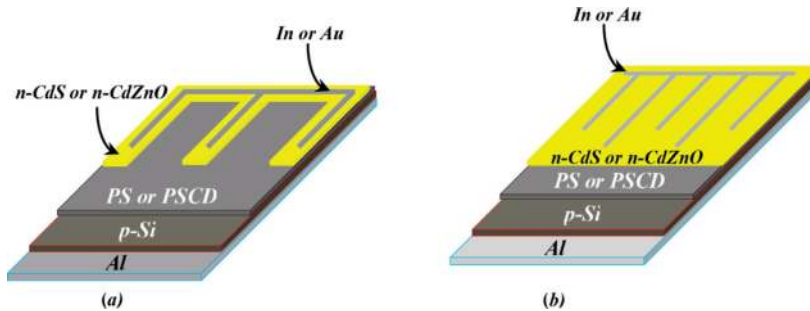


**Figure 1.**  
 Schematic structure of gas sensors (a) and solar cells (b) on the basis of PS and PSCD

voltammograms were scanned in the potential range from 1.2 to -1.2 V with the graphite (or Ag/AgCl) electrodes. Depending on the deposition time and pore size of the substrate, the 100–600-nm-thick CdS and Cd<sub>0.4</sub>Zn<sub>0.6</sub>O films with various surface morphologies were deposited. All the films showed n-type conductivity.

In order to fabricate the heterojunctions, an ohmic In (or Au) electrode, in grid form, was evaporated on the CdS and Cd<sub>0.4</sub>Zn<sub>0.6</sub>O films with an area of ~0.62 cm<sup>2</sup> (Figure 1). Aluminum (Al) was evaporated on the back side of the p-Si wafer as the ohmic electrode, followed by annealing at 500°C in a vacuum for 20 minutes.

### 3. Morphological, elemental, structural, and optical analyses

SEM images were obtained using a JEOL JSM-7600F and ZEISS Gemini 300 microscopes with energy dispersive spectroscopy (EDS) analysis.

Figure 2(a) illustrates the SEM images for PS surface formed at anodizing potential of 20 V, current of 10–40 mA/cm<sup>2</sup>, and time of 1800 sec. As can be seen from the figure, only nonhomogeneously distributed cavities are formed on the surface of the p-Si surface, after the anodizing in solution without CdCl<sub>2</sub>. Only in some parts of the surface appear the pore cores.

EDS spectrum shows a very small amount of hydrogen in the surface of these samples (Figure 2(b)). This fact proves only electropolishing of the c-Si surface in HF + H<sub>2</sub>O + ethanol solution at low anode potentials.

Unlike that, SEM images for PSCD layers, formed at anodizing potential of 20 V and current of 40 mA/cm<sup>2</sup> in HF + CdCl<sub>2</sub> + H<sub>2</sub>O + ethanol solution, show pores with very small dimension on the surface (Figure 3(a)). EDS spectrums confirm that Cd and hydrogen are on the surface of the layers (Figure 3(b)). The results show that Cd<sup>2+</sup> ions together with Si<sup>2+</sup> participate in charge exchange and accelerate the formation of initial growing piths on c-Si surface.

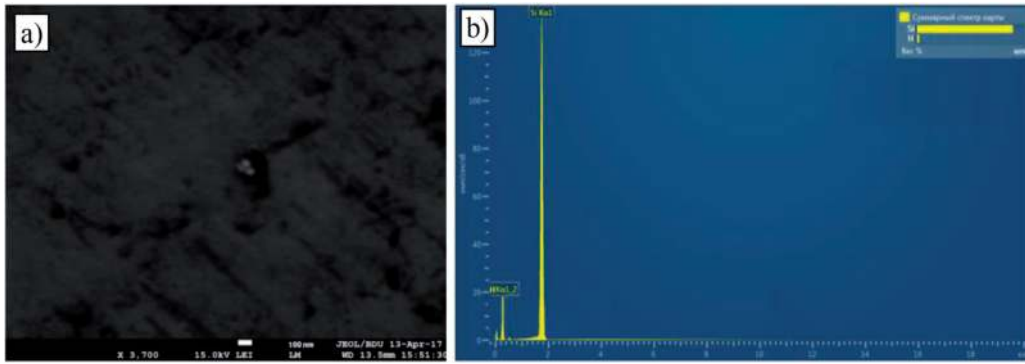


**Figure 2.** SEM image (a) and EDS spectrum (b) of the PS samples prepared at anodizing voltage of 20 V and current of 40 mA/cm<sup>2</sup>.

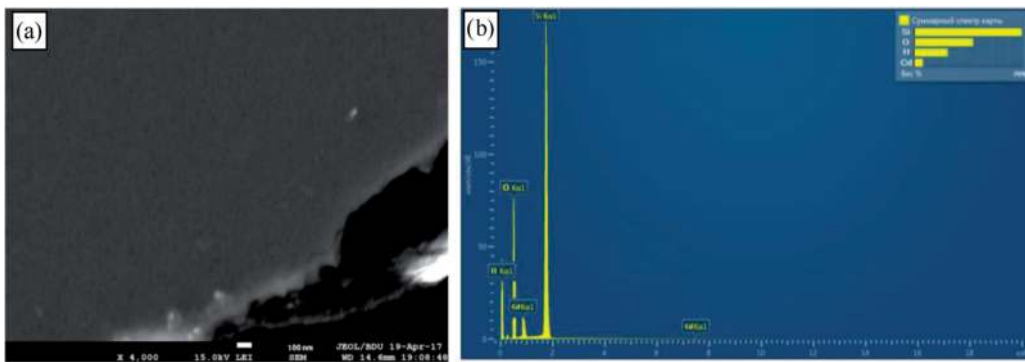


**Figure 3.** SEM image (a) and EDS spectrum (b) of the PSCD samples prepared at anodizing voltage of 20 V and current of 40 mA/cm<sup>2</sup>.

As a result, along with Si, cadmium atoms also deposit at the bottom and inside walls of the pores, causing the reduction of non-stable Si-H<sub>x</sub> bond concentration and their replacement by Si-Cd bonds. Subsequently, the neutralizing Cd atoms in the pores as a result of the charge exchange determine the structure of the pores. EDS spectrum of PSCD layers indicates the presence of Cd atoms on the pores.

Increasing the anode potential up to 25–30 V (at current of 10–40 mA/cm<sup>2</sup>) changes the nature of the anodizing—formation of pores is accelerating. SEM images show oval or spherical pores, which are distributed nonhomogeneously on the surface for PS samples (**Figure 4(a)**). The average dimensions of spherical-shaped pores were about 7–30 nm, and dimensions of oval-shaped pores were about 10–110 nm. Distribution of such pores on PS surface may be due to an irregular distribution of the anode current at Si-electrolyte boundary or relative weakening of the Si<sup>2+</sup> ion neutralization process because of “charge deficiency” in certain parts of the surface.

EDS spectrums show the oxygen in PS layers after keeping in the open air (**Figure 4(b)**). True, the PS samples also have Si-H<sub>x</sub> bonds, but the unstable bonds lead to degradation of parameters of the devices (gas sensors and solar cells). Si-O<sub>x</sub> bond leads also to an increase of the PS resistivity.

SEM investigations show that, unlike PS layers, pores in PSCD layers, prepared at anodizing voltage of 30 V, are distributed homogeneously and almost show spherical form cavities (**Figure 5(a)**). The subsequent increase of anode voltage (up to 40 V) almost does not change the size (**Table 2**) and shape of the pores. This fact shows that the Cd<sup>2+</sup> ions promote a uniform distribution of charges and anode voltage across the entire surface at the silicon-electrolyte interface. Uniform

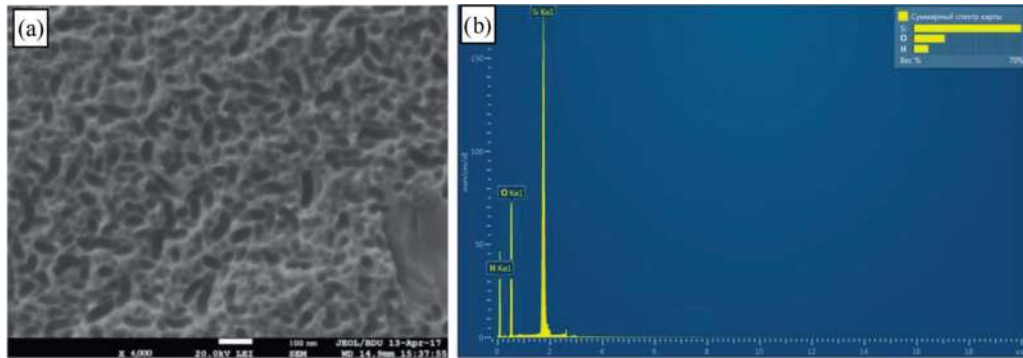


**Figure 4.** SEM image (a) and EDS spectrum (b) of the PS samples prepared at anodizing voltage of 30 V and current of 40 mA/cm<sup>2</sup>.

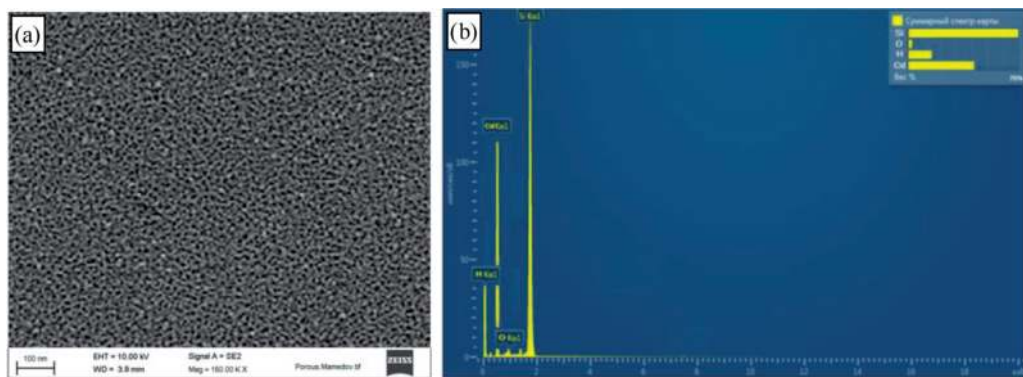


**Figure 5.** SEM image (a) and EDS spectrum (b) of the PSCD samples prepared at anodizing voltage of 30 V and current of 40 mA/cm<sup>2</sup>.

Samples	Anodizing voltage (V)	Anodizing current density (mA/cm <sup>2</sup> )	Anodizing time (s)	Pore sizes (nm)
PSCD1	30	40	1800	8÷11
PSCD2	30	55	1800	10÷16
PSCD3	30	70	1800	30÷70
PSCD2	34	55	1800	10÷15
PSCD2	36	55	1800	11÷17
PSCD2	40	55	1800	10÷19
PSCD2	30	55	1200	9÷16
PSCD2	30	55	400	10÷17

**Table 2.** Anodizing parameters of PSCD layers.

distribution of voltage on the silicon surface results in formation of pores with spherical shape. It is established that the size of the pores can be regulated only by anodizing current (Table 2). EDS spectrums testify an increase of Cd and a decrease of oxygen concentrations in the pores (Figure 5(b)).

It was possible to increase the size of the pores to 70–80 nm by increasing the anode current up to 70 mA/cm<sup>2</sup> (Figure 6(a) and (b)). It should also be noted that with the increase of the anode current, the location degree of Cd atoms in the pores



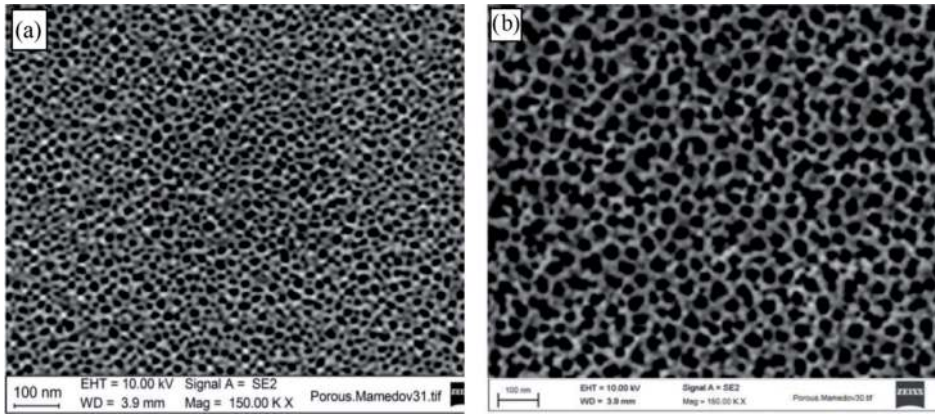


**Figure 6.** SEM images of PSCD samples prepared at anodizing voltage of 30 V and currents of 55 mA/cm<sup>2</sup> (a) and 70 mA/cm<sup>2</sup> (b).

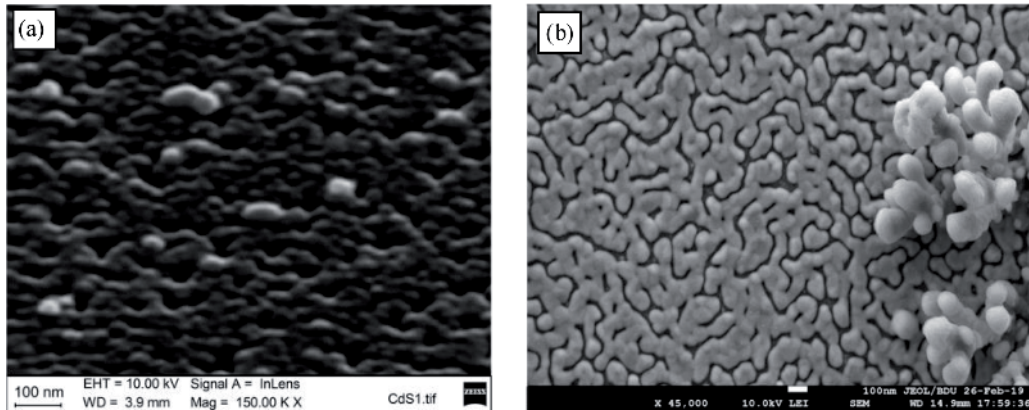


**Figure 7.** SEM images and AFM images of CdS (a) and Cd<sub>0.4</sub>Zn<sub>0.6</sub>O (b) films deposited on c-Si/PSCD<sub>1</sub> substrates.

also varies. Thus, EDS spectrums testify an increase of Cd and a decrease of oxygen concentrations in the pores, with increasing the anode current up to 55–60 mA/cm<sup>2</sup>. This fact shows that the low concentration of Si-O<sub>x</sub> bonds is formed in the pores, i.e., the most of Si-H<sub>x</sub> bonds are replaced by Si-Cd bonds (**Figure 5(b)**). Note that those EDS spectrums were drawn for samples immediately after depositing and after saving 1 month. In both cases, the same result is obtained—oxygen concentration in the pores has not changed. This also indicates that the PSCD layers prepared in metal ionic environment (in HF + CdCl<sub>2</sub> + ethanol solution) are stable.

But, further increase in current value up to 70 mA/cm<sup>2</sup> leads to the decrease of concentration of the Cd atoms and increase of oxygen concentration, as confirmed by EDS studies. However, Si-O<sub>x</sub> bonds are not stable and show variable valence, which allows the use of PSCD layers as sensors of various types of gases.

SEM and AFM images confirmed that the morphological properties of CdS and Cd<sub>0.4</sub>Zn<sub>0.6</sub>O films are governed by the pore size of PS. SEM images of thin films CdS (deposited at potential −0.82 V [19, 20]) and Cd<sub>0.4</sub>Zn<sub>0.6</sub>O (deposited at potential −1.2 V [21]) onto the c-Si/PSCD (PSCD1, PSCD2, and PSCD 3) are shown in **Figures 7–9**, respectively. As seen from figures, the size of crystallites of the CdS and Cd<sub>0.4</sub>Zn<sub>0.6</sub>O films can be controlled by selecting the pore size of silicon. The films deposited onto the substrate PSCD1 shows micro-texture structure. The grain sizes were ~20–70 μm for CdS films, and films of Cd<sub>0.4</sub>Zn<sub>0.6</sub>O show mosaic micro-crystalline (~0.12–150 μm) structure with some defects.

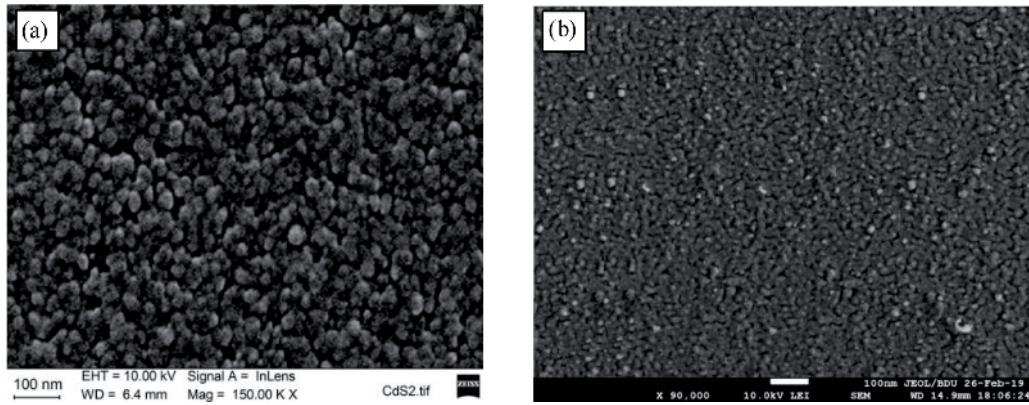


**Figure 8.** SEM images and AFM images of CdS (a) and Cd<sub>0.4</sub>Zn<sub>0.6</sub>O (b) films deposited on c-Si/PSCD<sub>2</sub> substrates.

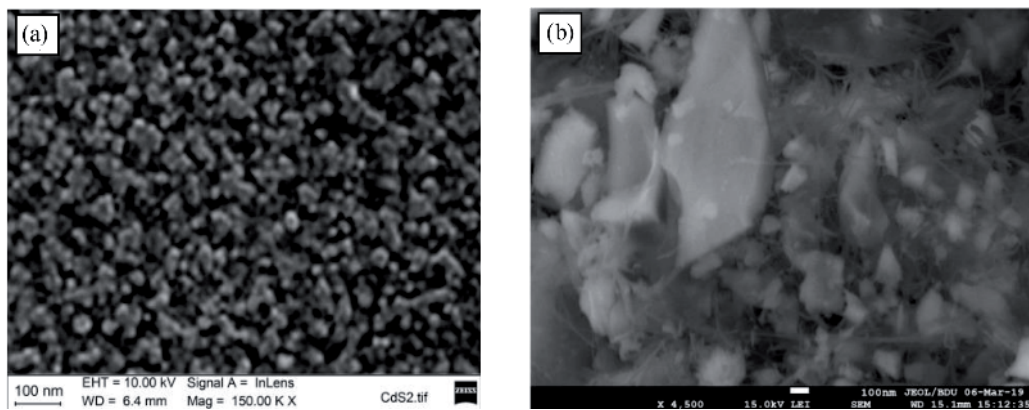


**Figure 9.** SEM images and AFM images of CdS (a) and Cd<sub>0.4</sub>Zn<sub>0.6</sub>O (b) films deposited on c-Si/PSCD<sub>3</sub> substrates.

As seen from **Figure 8**, when PSCD<sub>2</sub> is used as substrate, the size of the nanograins gets reduced due to the controlled process of nucleation, and nano-size grains are uniformly distributed at the surface. The size of particles, as determined by SEM, is found as 80–190 nm for CdS and 10–40 nm for Cd<sub>0.4</sub>Zn<sub>0.6</sub>O films.

The morphology of the films changes dramatically, when replacing substrates of PSCD<sub>2</sub> with PSCD<sub>3</sub> (with a pore size of 30 nm), since the crystallite sizes in both films increase and their uneven distribution is observed from SEM images (**Figure 9**). The size of the grains was different from each other, indicating irregular growth rate of the grains.

The crystal phase structure of films CdS and Cd<sub>0.4</sub>Zn<sub>0.6</sub>O was analyzed with a Shimadzu XRD-6100 diffractometer. X-ray diffraction patterns of Cd<sub>0.4</sub>Zn<sub>0.6</sub>O and CdS films deposited on glass/SnO<sub>2</sub> substrates confirm that they possess a hexagonal wurtzite and cubic structures, respectively. Cd<sub>0.4</sub>Zn<sub>0.6</sub>O films have a polycrystalline structure with a strongly preferred (002) c-axis orientation (as evidenced by the high intensity of the (002) diffraction peak). X-ray diffraction pattern of the CdS films shows peaks at 27, 44, and 52° corresponding to the planes (111), (220), and (311), respectively. The d-spacing values obtained match those of the corresponding reference material (JCPDS card No. 36-1451 for Cd<sub>0.4</sub>Zn<sub>0.6</sub>O and No. 10-0454 for CdS films) well.

The optical transmission spectrums were recorded with an Evolution 300 spectrophotometer. The band gap of Cd<sub>0.4</sub>Zn<sub>0.6</sub>O and CdS films was determined by extrapolating the straight-line section of the  $(\alpha h\nu)^2$  versus  $h\nu$  curves. The band gap of the Cd<sub>0.4</sub>Zn<sub>0.6</sub>O and CdS films was estimated to be 2.95 and 2.41 eV, respectively.

#### 4. Electrical characterization and gas sensitivity of p-Si/PS/CdS and p-Si/PS/Cd<sub>0.4</sub>Zn<sub>0.6</sub>O heterojunctions

Electrical properties of heterojunctions were studied depending on the crystallite and pore size. Current-voltage ( $J$ - $V$ ) characteristics show that all heterojunctions possess rectifying properties. The rectification factor and current passage mechanism through the junction region depends strongly on the pore and crystallite size. **Figure 10** represents the  $J$ - $V$  characteristics for as-deposited heterojunctions of p-Si/PSCD/CdS and p-Si/PSCD/Cd<sub>0.4</sub>Zn<sub>0.6</sub>O based on PSCD1, PSCD2, and PSCD3 substrates. The pass direction corresponds to positive polarity of the external bias on the  $c$ -Si layers.

The rectification at  $U = 1$  V increases from 2340 to 4670 for  $c$ -Si/PSCD/CdS and from 780 to 1650 for  $c$ -Si/PSCD/Cd<sub>0.4</sub>Zn<sub>0.6</sub>O heterojunctions, when replacing the PSCD1 substrates with PSCD2. As seen from **Table 3**, rectification in both types of heterojunctions is decreased sharply, when PSCD3 is used as substrate. It is assumed that the change in rectification factor value depending on the pore size is due to the oxygen or nitrogen molecules, because in order to remove excess water from pores and films, heterojunctions were dried in air, just after the deposition (as-deposited heterojunctions). In this case, adsorbed oxygen or nitrogen molecules to the silicon pores (mainly for PSCD3 substrates) create the acceptor states in junction region and thus increase recombination acts. It is established that the degree of adsorption depends on pore size. To confirm this fact, heterojunctions were heat-treated in a vacuum at 50–70°C, and  $J$ - $V$  characteristics were taken in a vacuum. It is established that the rectification in heterojunctions deposited onto the PSCD2 substrates remained almost unchanged (**Table 4**). But the rectification in both types of heterojunctions on the base of PSCD3 substrates increases sharply, which, by our opinion, is due to desorption of oxygen or nitrogen molecules (**Table 4**).

To prove this, we carried out additional experiments on these heterojunctions. Direct current at  $U = 1$  V was measured in air with different concentrations. Direct current in heterojunctions with PSCD2 has not changed and in heterojunctions with PSCD3 decreased with increasing air concentration (**Figure 11**).

Dependences of direct current at  $U = 1$  V for heterojunctions with PSCD1, PSCD2, and PSCD3, on the concentration of various gases (oxygen, nitrogen, methane, and ethanol vapor), have been investigated. As seen from **Figure 12**, the direct current decreases at an insignificant change of the gas concentration. It is suggested that heterojunctions with PSCD3 can be used as gas sensors.

Experiments carried out in various atmospheres on heterojunctions with PSCD1 showed insignificant changes of current, and junctions with PSCD2 do not show

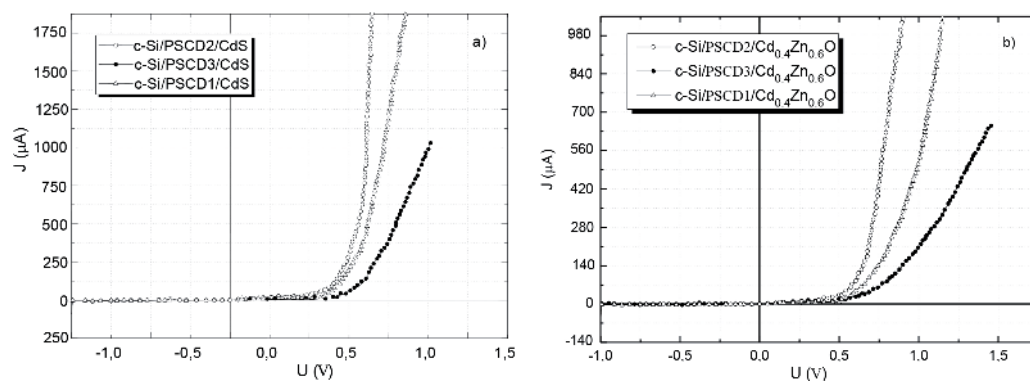


**Figure 10.**

Dark  $J$ - $V$  curves for as-deposited  $c$ -Si/PSCD/CdS and  $c$ -Si/PSCD/Cd<sub>0.4</sub>Zn<sub>0.6</sub>O heterojunctions prepared onto the PSCD1, PSCD2, and PSCD3 substrates.



Samples	Substrates	Ideality factor	Rectification factor
c-Si/PSCD/CdS	PSCD1	1.5	2340
	PSCD2	1.24	4670
	PSCD3	2.67	1076
c-Si/PSCD/Cd <sub>0.4</sub> Zn <sub>0.6</sub> O	PSCD1	1.66	780
	PSCD2	1.35	1650
	PSCD3	2.84	240

**Table 3.**  
 Electrical parameters of c-Si/PSCD/CdS and c-Si/PSCD/Cd<sub>0.4</sub>Zn<sub>0.6</sub>O as-deposited heterojunctions depending on the pore size in Si.

Samples	Substrates	Ideality factor	Rectification factor
c-Si/PSCD/CdS	PSCD1	1.5	2346
	PSCD2	1.24	4680
	PSCD3	1.63	1954
c-Si/PSCD/Cd <sub>0.4</sub> Zn <sub>0.6</sub> O	PSCD1	1.66	785
	PSCD2	1.35	1670
	PSCD3	1.75	1087

**Table 4.**  
 Electrical parameters of heterojunctions c-Si/PSCD/CdS and c-Si/PSCD/Cd<sub>0.4</sub>Zn<sub>0.6</sub>O heat-treated in a vacuum at 50–70°C, depending on the pore size in Si.

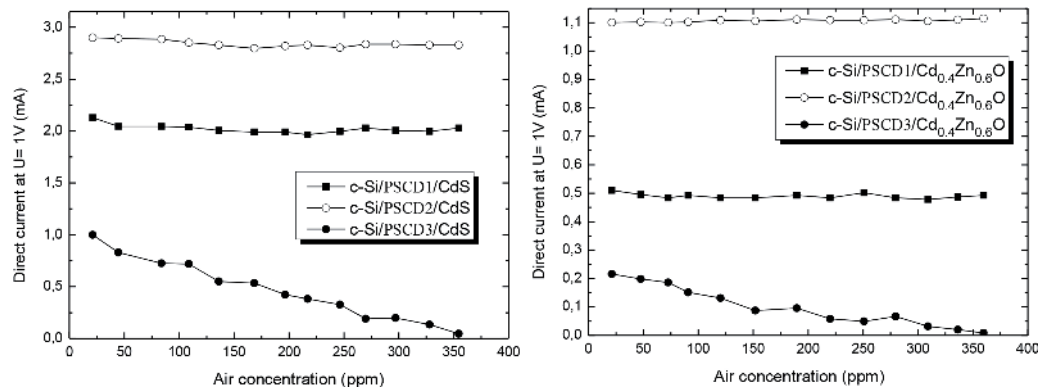


**Figure 11.**  
 Dependence of direct current at  $U = 1$  V on the air concentration for as-deposited heterojunctions of c-Si/PSCD/CdS and c-Si/PSCD/Cd<sub>0.4</sub>Zn<sub>0.6</sub>O with different pore size.

any changes of direct current, i.e., they have stable parameters. This fact testifies that heterojunctions with PSCD1 and PSCD2 can be used for manufacturing solar cells.

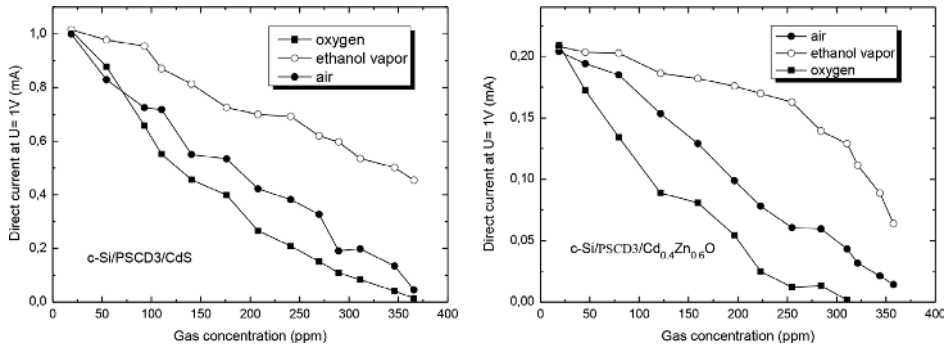


**Figure 12.** Dependence of direct current at  $U = 1\text{ V}$  on the concentration of different gases for heterojunctions  $c\text{-Si/PSCD}_3/\text{CdS}$  and  $c\text{-Si/PSCD}_3/\text{Cd}_{0.4}\text{Zn}_{0.6}\text{O}$ .

The  $J$ - $V$  characteristics of heterojunctions with PSCD1 and PSCD2, in natural log scale and temperature dependences of diode saturation current, testify that there is a tunnel-recombination mechanism of current through the junction region at direct voltages, and  $J$ - $V$  characteristics of these heterojunctions can be presented by expression:

$$J = J_0 \left[ \exp\left(\frac{eU}{nkT}\right) - 1 \right] \quad (1)$$

Here,  $J_0$  is the saturation current density,  $U$  is the applied voltage,  $e$  is the electron charge,  $n$  is the ideality factor,  $k$  is the Boltzmann constant, and  $T$  is the temperature.

At room temperature the ideality factor values for heterojunctions with PSCD1 were approximately 1.5 and 1.66, respectively, for the heterojunctions  $c\text{-Si/PSCD1/CdS}$  and  $c\text{-Si/PSCD1/Cd}_{0.4}\text{Zn}_{0.6}\text{O}$ . The decrease of ideality factor has been observed when PSCD2 substrates is used (Table 4).

Figure 13 shows the room temperature capacitance-voltage ( $C$ - $V$ ) characteristics of heterojunctions  $c\text{-Si/PSCD/CdS}$  and  $c\text{-Si/PSCD/Cd}_{0.4}\text{Zn}_{0.6}\text{O}$ , with PSCD1 and PSCD2 substrates. The linearity of the  $C$ - $V$  characteristics in  $C^{-2}$  ( $V$ ) coordinates indicates a sharp distribution of uncompensated acceptor impurities within the space charge region for both types of heterojunctions with PSCD2. Unlike it,  $C$ - $V$  characteristics of heterojunctions  $c\text{-Si/PSCD/CdS}$  and  $c\text{-Si/PSCD/Cd}_{0.4}\text{Zn}_{0.6}\text{O}$ , with PSCD1 substrates, have peculiarities, typical for heterojunctions with the presence of defects at the junction region. Since the  $C$ - $V$  characteristics of these junctions are poorly linearized in  $C^{-2}$  ( $V$ ) coordinates, its slope changes by frequency of the alternating signal.

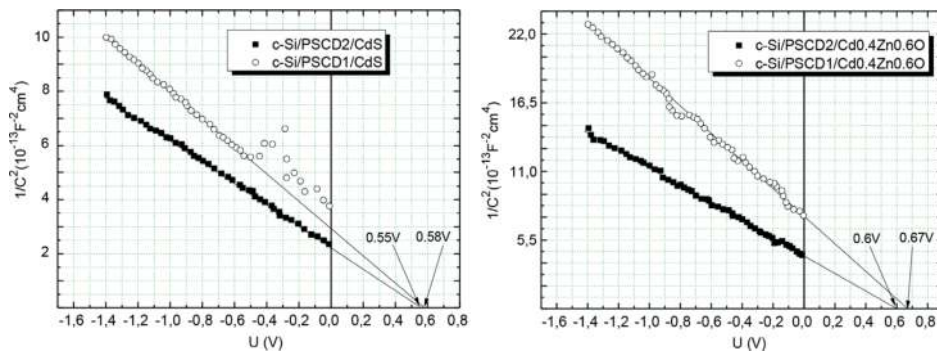


**Figure 13.** Capacitance-voltage characteristics of heterojunctions  $c\text{-Si/PSCD/CdS}$  and  $c\text{-Si/PSCD/Cd}_{0.4}\text{Zn}_{0.6}\text{O}$  based on PSCD1 and PSCD2 substrates

As seen from the figures, the value of cutoff voltage ( $V_c$ ) is greater than heterojunctions based on PSCD2 substrates. It can be explained by the participation of oxygen (as Si-O<sub>x</sub> bonds) on the surface of PSCD1 substrates, which can form the oxide layer (as CdO or Cd<sub>1-x</sub>Zn<sub>x</sub>O) between the porous silicon and CdS (Cd<sub>1-x</sub>Zn<sub>x</sub>O) films. This is confirmed by the frequency dependence of straight sections of the  $C^{-2}(V)$  slopes, which indicates an increase of heterojunction capacity with increasing frequency.

### 5. Photosensitivity of p-Si/PS/CdS and p-Si/PS/Cd<sub>0.4</sub>Zn<sub>0.6</sub>O heterojunctions

The simulated  $J$ - $V$  characteristics under AM1.5 sunlight exposure show the higher photovoltaic performance of the heterojunctions c-Si/PSCD/CdS and c-Si/PSCD/Cd<sub>0.4</sub>Zn<sub>0.6</sub>O based on PSCD substrates. As shown from these investigations, the sign of open circuit photovoltage ( $U_{oc}$ ) does not change in all regions of photosensitivity. However, the values of  $U_{oc}$  and  $J_{sc}$  are non-monotonically dependent on the type of PSCD—maximum photosensitivity shows the heterojunctions based on PSCD2 substrates (Figure 14).

Spectral distribution of photocurrent ( $J_{ph}$ ) in heterojunctions c-Si/PSCD/CdS and c-Si/PSCD/Cd<sub>0.4</sub>Zn<sub>0.6</sub>O with different types of PSCD was investigated in a wavelength range of 300–1300 nm (Figure 15). It is established that the profile of  $J_{ph}$  spectrum depends on the pore size and morphology of CdS and Cd<sub>0.4</sub>Zn<sub>0.6</sub>O films. As seen from the figure, short-wavelength peak for heterojunctions c-Si/PSCD/CdS and c-Si/PSCD/Cd<sub>0.4</sub>Zn<sub>0.6</sub>O based on PSCD1 is observed, respectively, at

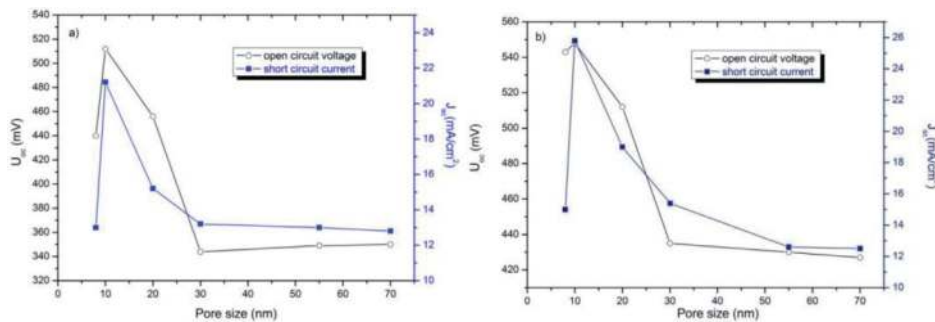


**Figure 14.** Dependences of  $U_{oc}$  and  $J_{sc}$  on the pore size in silicon for heterojunctions c-Si/PSCD/Cd<sub>0.4</sub>Zn<sub>0.6</sub>O (a) and c-Si/PSCD/CdS (b).

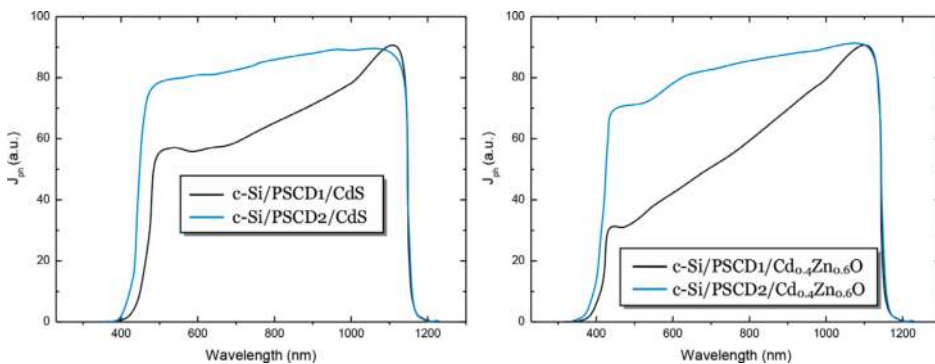


**Figure 15.** Spectral distribution of photocurrent for heterojunctions c-Si/PSCD/CdS and c-Si/PSCD/Cd<sub>0.4</sub>Zn<sub>0.6</sub>O based on PSCD1 and PDCS2 substrates [19–22].

Samples	Substrates	$U_{oc}$ , mV	$J_{sc}$ , mA/cm <sup>2</sup>	FF	$\eta$ , %
c-Si/PSCD/CdS	PSCD1	543	15	0.62	5.05
	PSCD2	548	25.8	0.68	9.61
	PSCD3	435	15.4	0.6	4.01
c-Si/PSCD/Cd <sub>0.4</sub> Zn <sub>0.6</sub> O	PSCD1	440	13	0.55	3.15
	PSCD2	512	21.2	0.61	6.62
	PSCD3	344	13.2	0.52	2.36

**Table 5.**

Photoelectrical parameters of heterojunctions c-Si/PSCD/CdS and c-Si/PSCD/Cd<sub>0.4</sub>Zn<sub>0.6</sub>O heat-treated in a vacuum at 50–70°C, depending on the pore size in Si.

510 and 420 nm, which corresponds to the band gap of CdS and Cd<sub>0.4</sub>Zn<sub>0.6</sub>O films. However, long-wavelength peak of spectrum at 1125 nm is due to the direct inter-band transitions in c-Si. It can be seen from **Figure 15** that heterojunctions of c-Si/PSCD/CdS and c-Si/PSCD/Cd<sub>0.4</sub>Zn<sub>0.6</sub>O demonstrate a good photo response in the wavelength range of 512–1125 nm and 425–1125 nm, which is not observed by us in heterojunctions of c-Si/A<sub>2</sub>B<sub>6</sub> [23].

It is assumed that this is due to light absorption in porous silicon. The slight shifting of a short-wavelength peak in both type of heterojunctions to the more short-wavelength region of the spectrum, with increasing pores size (for PSCD2), is associated by us with the nano-structural properties of CdS and Cd<sub>0.4</sub>Zn<sub>0.6</sub>O films [19–22]. However, an increase of the optical path of light in nanostructured films leads to an increase of degree of the light absorption; therefore, heterojunctions based on PSCD2 show greater efficiency compared to heterojunctions based on PSCD1 (**Table 5**).

## 6. Conclusions

Gas and photo sensors based on c-Si/PS (or PSCD)/CdS and c-Si/PS/Cd<sub>0.4</sub>Zn<sub>0.6</sub>O heterojunctions were fabricated by electrodepositing CdS and Cd<sub>0.4</sub>Zn<sub>0.6</sub>O films onto the c-Si/PS (or PSCD) substrates. SEM images confirmed that the morphological properties of CdS and Cd<sub>0.4</sub>Zn<sub>0.6</sub>O films are governed by the pore size of PS and PSCD. The higher gas and photo sensitivities in heterojunctions based on PSCD were achieved when the pore sizes were 30 and 10 nm, respectively. The pronounced PS pore diameter and anodizing regime dependence of the photo- and gas sensitivity are the main novelty of the present work. We believe that this phenomenon could be exploited in other similar heterojunction types and even in hybrid solar cells containing, e.g., a perovskite charge separation layer.




## **Author details**

Huseyn M. Mamedov  
Faculty of Physics, Department of Physical Electronics, Baku State University,  
Baku, Azerbaijan

\*Address all correspondence to: [mhhuseyng@bsu.edu.az](mailto:mhhuseyng@bsu.edu.az)

## **IntechOpen**

© 2020 The Author(s). Licensee IntechOpen. Distributed under the terms of the Creative Commons Attribution - NonCommercial 4.0 License (<https://creativecommons.org/licenses/by-nc/4.0/>), which permits use, distribution and reproduction for non-commercial purposes, provided the original is properly cited. 

## References

- [1] Nalin HM, Jibinlal A, Divesh NS. Application of porous silicon in solar cell. In: Proceedings of International Conference on Nanomaterials for Energy Conversion and Storage Applications (NECSA 2018). Gujarat, India: AIP Publishing; 29-31 January 2018; **1961**:030019-030022. DOI: 10.1063/1.5035221
- [2] Giuseppe B. Porous silicon gas sensing. In: Canham L, editor. Handbook of Porous Silicon. 2nd ed. Switzerland: Springer; 2014. pp. 1251-1262. Available from: <https://doi.org/10.1007/978-3-319-71381-6>
- [3] Santinacci L, Gonçalves A, Simon N, Etcheberry A. Electrochemical and optical characterizations of anodic porous n-InP(1 0 0) layers. *Electrochimica Acta*. 2010; **56**:878-888. DOI: 10.1016/j.electacta.2010.09.031
- [4] Raid AI, Alwan MA, Ahmed SA. Preparation and characteristics study of nano-porous silicon UV photodetector. *Applied Nanoscience*. 2016; **7**:9-15. DOI: 10.1007/s13204-016-0544-9
- [5] Naser MA, Al-Dourib Y, Alwan MA, Allaa AJ, Ghassan EA. Characteristics of nanostructure silicon photodiode using laser assisted etching. *Procedia Engineering*. 2013; **53**:393-399. DOI: 10.1016/j.proeng.2013.02.051
- [6] Oh D, Kim TW, Cho W, Kwack KD. Effects of a H<sub>2</sub>SO<sub>4</sub> treatment on the optical properties in porous Si layers and electrical properties of diode devices fabricated with a H<sub>2</sub>SO<sub>4</sub> treated porous Si layer. *Journal of Ceramic Processing Research*. 2008; **9**:57-60
- [7] Granitzer P, Rumpf K. Porous silicon—A versatile host material. *Materials*. 2010; **3**:943-998. DOI: 10.3390/ma3020943
- [8] Korotcenkov G. Porous Silicon: From Formation to Application. Vol. 1: Formation and Properties. Taylor and Francis Group: CRC Press; 2015. p. 432. DOI: 10.1201/b19342
- [9] Korotcenkov G. Porous Silicon: From Formation to Application. Vol. 2: Biomedical and Sensor Applications. Taylor and Francis Group: CRC Press; 2016. p. 424. DOI: 10.1201/b19342
- [10] Korotcenkov G, editor. Porous Silicon: From Formation to Application. Vol. 3: Microelectronics, Optoelectronics and Energy Technology Applications. Taylor and Francis Group: CRC Press; 2016. p. 430. DOI: 10.1201/b19342
- [11] Venger EF, Holiney RY, Matveeva LA, Vasin AV. The influence of hydrogen plasma on the spectrum of electromotive reflections and the spectrum of electronic states of porous silicon. *Semiconductors*. 2003; **37**:103-107
- [12] Sreseli OM, Goryachev DN, Osipov VY, Belyakov LV, Vul SP, Serenkov IT, et al. Preparation and study of carbidized porous silicon. *Semiconductors*. 2002; **36**:574-580
- [13] Primachenko VE, Kononets JF, Bulakh BM, Venger EF, Kaganovich ÉB, Kizyak IM, et al. The electronic and emissive properties of Au-doped porous silicon. *Semiconductors*. 2005; **39**:565-571
- [14] Shevchenko OY, Goryachev DN, Belyakov LV, Sresli OM. Optical properties of iron-passivated nanoporous silicon. *Semiconductors*. 2010; **44**:642-646
- [15] Xu YK, Adachi S. Properties of light-emitting porous silicon photoetched in

aqueous HF/FeCl<sub>3</sub> solution. *Journal of Applied Physics*. 2007;**101**(10):103509. DOI: 10.1063/1.2733752

[16] Xu YK, Adachi S. Properties of light-emitting porous silicon formed by stain etching in HF/KIO<sub>3</sub> solution under light illumination. *Journal of Applied Physics*. 2008;**103**(10):103512. DOI: 10.1063/1.2924423

[17] Fathauer RW, George T, Ksendzov A, Vasquez RP. Visible luminescence from silicon wafers subjected to stain etches. *Applied Physics Letters*. 1992;**60**(8):995-997. DOI: 10.1063/1.106485

[18] Karbassian F. Porous Silicon. In: Taher G, editor. *Porosity - Process, Technologies and Applications*. UK: IntechOpen; 2018. p. 1-36. DOI: 10.5772/intechopen.68404

[19] Mamedov HM, Muradov MB, Konya Z, Kukovecz A, Kordas K, Shah SI, et al. Fabrication and characterization of c-Si/porous-Si/CdS/Zn<sub>x</sub>Cd<sub>1-x</sub>O heterojunctions for applications in nanostructured solar cells. *Photonics Letters of Poland*. 2018;**10**:73-75. DOI: 10.4302/plp.v10i3.813

[20] Mamedov HM, Kukevecz A, Konya Z, Kordas K, Shah SI, Mamedov VU, et al. Characteristics of c-Si/porous-Si/CdS heterojunctions. *News of higher educational institutions. Physics (Russian Journal of Applied Physics)*. 2018;**61**:96-101. DOI: 10.1007/s11182-018-1584-2

[21] Mamedov HM, Mamedov VU, Mamedova VJ, Ahmedova KM, Tagiyev EB, Agazade LE. Nano-structure solar cells on the base of p-Si/Cd<sub>1-x</sub>Zn<sub>x</sub>O thin film heterojunctions. *Journal of Optoelectronics and Advanced Materials*. 2018;**20**:468-473

[22] Mamedov HM, Shah SI, Chirakadze A, Mamedov VU, Mamedova VJ,

Ahmedova KM. Photovoltaic performance of p-Si/Cd<sub>1-x</sub>Zn<sub>x</sub>O heterojunctions. *Photonics Letters of Poland*. 2018;**10**:26-28. DOI: 10.4302/plp.v10i1.797

[23] Abdinov AS, Mamedov HM, Hasanov HA, Amirova SI. Photosensitivity of p, n-Si/n-Cd<sub>1-x</sub>Zn<sub>x</sub>S heterojunctions manufactured by a method of electrochemical deposition. *Thin Solid Films*. 2005;**480-481**:388-391